35th Annual International Conference of the IEEE EMBS
Osaka, Japan, 3 - 7 July, 2013

Identification of Recurring Wavefront Propagation Patterns in Atrial Fibrillation using Basis Pursuit*

S. Zeemering[1], R. Peeters[2], A. van Hunnik[1], S. Verheule[1], U. Schotten[1]

Abstract— **High density contact electrogram data of atrial fibrillation (AF) contain detailed information on recurring activation patterns and dominant signaling pathways. Current methods to analyze these patterns and pathways rely mainly on supervised atrial deflection annotation and wave reconstruction. In this study, we developed a new algorithm to automatically identify recurring patterns and dominant pathways without the need for annotation. A sparse multivariate autoregression model was estimated on short segments of synchronous unipolar electrograms to extract the dominant interactions between electrograms at different recording electrodes. Sparsity of the electrode interaction matrices at several time-lags was maximized by applying a distance-weighted basis pursuit algorithm. Dominant interactions were identified by computing the mean interaction matrix over a number of consecutive time segments. The algorithm was evaluated on high-density recordings with 234 electrodes and 2.4mm electrode spacing in the left and right atrial free wall of a goat model of AF. The method was able to identify relevant patterns of AF, including wave trains, repetitive breakthrough waves and rotating wave activity.**

I. Introduction

The identification of recurring patterns in high-density recordings of atrial fibrillation (AF) provides valuable insight in the underlying mechanisms that determine the complexity of the AF substrate. Response to treatment of AF, whether this is for instance ablation therapy or pharmacological intervention, is dependent on this AF substrate complexity. High-density contact mapping of AF may give a good first visual impression of recurring wavefront patterns, but detailed substrate analysis requires extensive signal processing of atrial electrograms, atrial deflection detection and fibrillation wave reconstruction. We hypothesize that recurring patterns and signaling pathways can be identified using electrograms and electrode topology alone, employing a sparse multivariate autoregression (MVAR) modeling approach. A recent study showed that a similar approach can lead to meaningful results when identifying propagation patterns between several intracardiac recording sites using bipolar electrograms from a basket catheter [1]. In contrast to this approach, we intend to identify interactions between *unipolar* electrograms within a *short timeframe* to account for the dynamical nature of complex atrial fibrillation patterns. Furthermore, the spatial resolution of these unipolar recordings is higher (interelectrode distance 2.4mm) than in bipolar electrogram acquisition devices such as a basket catheter.

The MVAR model used in our approach allows us to choose 1) the maximum time-delay (the model order), 2) some dead time, and 3) model sparsity. The model order has to be chosen in such a way that sufficient but not too much past electrical activity is used to explain current activity. Including dead time is necessary to prevent (almost) simultaneous activations in a wavefront to be used to explain and detect spatial interaction in the direction of wave propagation. Sparsity is used to highlight dominant interactions. We are interested in spatial interactions, which is why we use an averaging procedure over time, within a suitably short window to prevent too many different wavefronts to cancel each other out. A key issue here is that otherwise unrelated atrial complexes often have similar morphology, so that any method that maximizes sparsity is prone to identify dominant interactions between unrelated locations. To address this issue we developed a distance-weighted adaptation of the basis pursuit algorithm [2] that maximizes the sparsity of the MVAR interaction matrices, while also regularizing sparsity based on interelectrode distance. The algorithm was then applied to a set of recordings in a goat model of AF that contained multiple recurrent wavefront propagation patterns.

II. Methods

A. Sparse multivariate autoregression model

The MVAR model of order P for a set of N synchronous recorded electrograms $\mathbf{x}[k] = [x_1[k], x_2[k], \ldots, x_N[k]]^T, k = 1, 2, \ldots, M$ with a dead time δ, can be formulated as

$$\mathbf{x}[k] = \sum_{\tau=\delta}^{\delta+P-1} \mathbf{A}_\tau \mathbf{x}[k-\tau] + \mathbf{w}[k], \qquad (1)$$

where each $\mathbf{A}_\tau$ is the $N \times N$ matrix with entries $a_{ij}(\tau)$ quantifying an interaction from $x_j[k-\tau]$ to $x_i[k]$. The vector $\mathbf{w}[k] = [w_1[k], w_2[k], \ldots, w_N[k]]$ is a multivariate white noise process. The model in (1) can be written in matrix form:

$$X = \Phi\Theta + W, \qquad (2)$$

*This study was supported by a grant from the Dutch Research Organization (NWO, VIDI-grant 016.086.379), a grant from the Foundation Leducq (07CVD03), and a grant from the European Union (FP7 Collaborative project EUTRAF, 261057).

[1]S. Zeemering, A. van Hunnik, S. Verheule and U. Schotten are with the Department of Physiology, Maastricht University, P.O. Box 616, 6200 MD, Maastricht, The Netherlands, +31 (0)43 388 1320, s.zeemering@maastrichtuniversity.nl

[2]R. Peeters is with the Department of Knowledge Engineering, Maastricht University, Maastricht, The Netherlands.

978-1-4577-0216-7/13/$26.00 ©2013 IEEE

where

$$X = [\mathbf{x}[\delta+P], \mathbf{x}[\delta+P+1], \ldots, \mathbf{x}[M]]^T$$
$$\Phi = \begin{bmatrix} \mathbf{x}[P] & \cdots & \mathbf{x}[M-\delta] \\ \vdots & \ddots & \vdots \\ \mathbf{x}[1] & \cdots & \mathbf{x}[M-(\delta+P-1)] \end{bmatrix}^T$$
$$\Theta = [\mathbf{A}_\delta, \mathbf{A}_{\delta+1}, \ldots, \mathbf{A}_{\delta+P-1}]^T$$
$$W = [\mathbf{w}[\delta+P], \mathbf{w}[\delta+P+1], \ldots, \mathbf{w}[M]]^T .$$

For a set of electrograms with $M \geq NP + \delta$ and Φ with full column rank NP, the unique least squares (LS) solution can be derived for each column $\theta^{(i)}$ of Θ separately

$$\theta_{LS}^{(i)} = \left(\Phi^T\Phi\right)^{-1}\Phi^T\mathbf{x}^{(i)}, \tag{3}$$

where $\mathbf{x}^{(i)}$ denotes column i of X. In this study we focus on short time-segments of electrograms, which typically causes the number (NP) of parameters that needs to be estimated for each column $\theta^{(i)}$ to be much larger than the available number of observations M. If the matrix Φ has rank $r < NP$, which necessarily happens if $M-\delta-P+1 < NP$, then there is no unique LS solution, but an optimal least squares solution space of dimension $NP-r$. This equivalence space with respect to the LS criterion can be exploited to maximize the sparsity of the parameter vector $\theta^{(i)}$. We apply a basis pursuit algorithm to find a parameter vector $\theta^{(i)}$ with minimal L_1-norm, while retaining the optimal least squares fit:

$$\min_{\theta^{(i)}} \|\theta^{(i)}\|_1 \quad \text{subject to } \Phi\theta^{(i)} = \Phi\theta_{LS}^{(i)}. \tag{4}$$

Minimizing the L_1-norm has been shown to produce a solution with maximum sparsity under certain conditions [3], even in the presence of noise [4]. Note that the right-hand side vector in the constraint in (4) is a unique vector, formed by the the orthogonal projection of $\mathbf{x}^{(i)}$ on the column space of Φ which does not depend on the choice of a solution in the equivalence space for the LS criterion.

An $N \times N$ spatiotemporal weight matrix C_τ can be defined and incorporated into the criterion function in (4) which allows to regularize sparsity at corresponding entries of $\mathbf{A}_\tau$. Define C as

$$C = [C_\delta, C_{\delta+1}, \ldots, C_{\delta+P-1}]^T, \tag{5}$$

and $C^{(i)}$ as column i of C. The regularized problem can now be written as

$$\min_{\theta^{(i)}} (C^{(i)})^T \left[|\theta_1^{(i)}|, |\theta_2^{(i)}|, \ldots, |\theta_{NP}^{(i)}|\right]^T$$
$$\text{subject to } \Phi\theta^{(i)} = \Phi\theta_{LS}^{(i)}, \tag{6}$$

The problem in (6) can be solved using linear programming by bringing it into standard form:

$$\min_{\theta^+,\theta^-} (C^{(i)})^T \left(\theta^+ + \theta^-\right)$$
$$\text{s.t. } \Phi(\theta^+ - \theta^-) = \Phi\theta_{LS}^{(i)}$$
$$\theta_i^+, \theta_i^- \geq 0 \quad i = 1, 2, \ldots, NP, \tag{7}$$

where $\theta^{(i)} = \theta^+ - \theta^-$. The resulting column vectors $\tilde{\theta}^{(i)}$ with minimal L_1-norm are joined to form the estimated matrix $\tilde{\Theta}$. From this matrix the estimated interaction matrices $\tilde{\mathbf{A}}_\tau$ can be constructed. To compute a solution $\theta_{LS}^{(i)}$ which features in (7), several approaches are possible. One is to employ the data directly as indicated in the definitions of Φ and X above and to use classical techniques from linear algebra such as QR-decomposition or an SVD-approach. However, the matrix $\Phi^T\Phi$ in the LS formula (3) is known to have a near block-Toeplitz structure which admits highly efficient recursive inversion. This is the basis for the well-known Levinson algorithm and its multivariate generalizations such as the Whittle-Wiggins-Robinson algorithm, see [6], which allow for the computation of an LS solution recursively in the order P of the MVAR model. This may speed up the estimation process, and it also allows one to use information theoretic criteria to select an appropriate value for P.

B. Dominant pathway identification

The goal of the sparse MVAR model estimation is to identify the dominant interactions between synchronous electrograms within a relatively short time interval of length M, typically shorter than one AF cycle length. A set of electrograms of duration $> M$ is analyzed by extracting L consecutive intervals of length M with overlap $M/2$ and estimating the sparse MVAR model for each of the intervals. The estimated MVAR model matrices $\tilde{\mathbf{A}}_\tau$ are then analyzed to extract information on recurring interaction patterns. We will focus on the regularization of spatial sparsity only and define the spatiotemporal weight matrix C_τ as

$$C_{\tau,ij} = \exp\left(\frac{d_{ij}}{\lambda}\right), \tau = \delta, \ldots, \delta+P-1, \tag{8}$$

where d_{ij} is the euclidean distance between electrodes i and j in millimeters and λ is a decay factor. The model coefficients are indicators of the strength of the interaction between two electrodes at a certain time delay, based on electrogram morphology. The mean interaction $\overline{a}_{ij}$from electrode j to i is defined as

$$\overline{a}_{ij} = \frac{\sum_{l=1}^{L}\sum_{\tau=\delta}^{\delta+P-1}\tilde{\mathbf{A}}(l)_{\tau,ij}}{PL}, \tag{9}$$

where $\tilde{\mathbf{A}}(l)_\tau$ denotes the interaction matrix $\tilde{\mathbf{A}}_\tau$ estimated on the interval l. Pathway maps are constructed from the mean electrode interaction matrix $\overline{\mathbf{A}}$.

C. High-density contact mapping

A subset of the mapping data presented in [5] was used for analysis. In short, goats were instrumented with an atrial endocardial pacemaker lead and a burst pacemaker. AF was maintained for 3 weeks (short-term AF [ST], n=10) or 6 months (long-term AF [LT], n=7). In an open-chest follow-up experiment, electrograms during AF were recorded from the left atrial (LA) and right atrial (RA) free walls using a round, high-density electrode array of 4cm in diameter, consisting of 234 unipolar recording electrodes with an interelectrode distance of 2.4mm (sampling rate 1kHz). Three

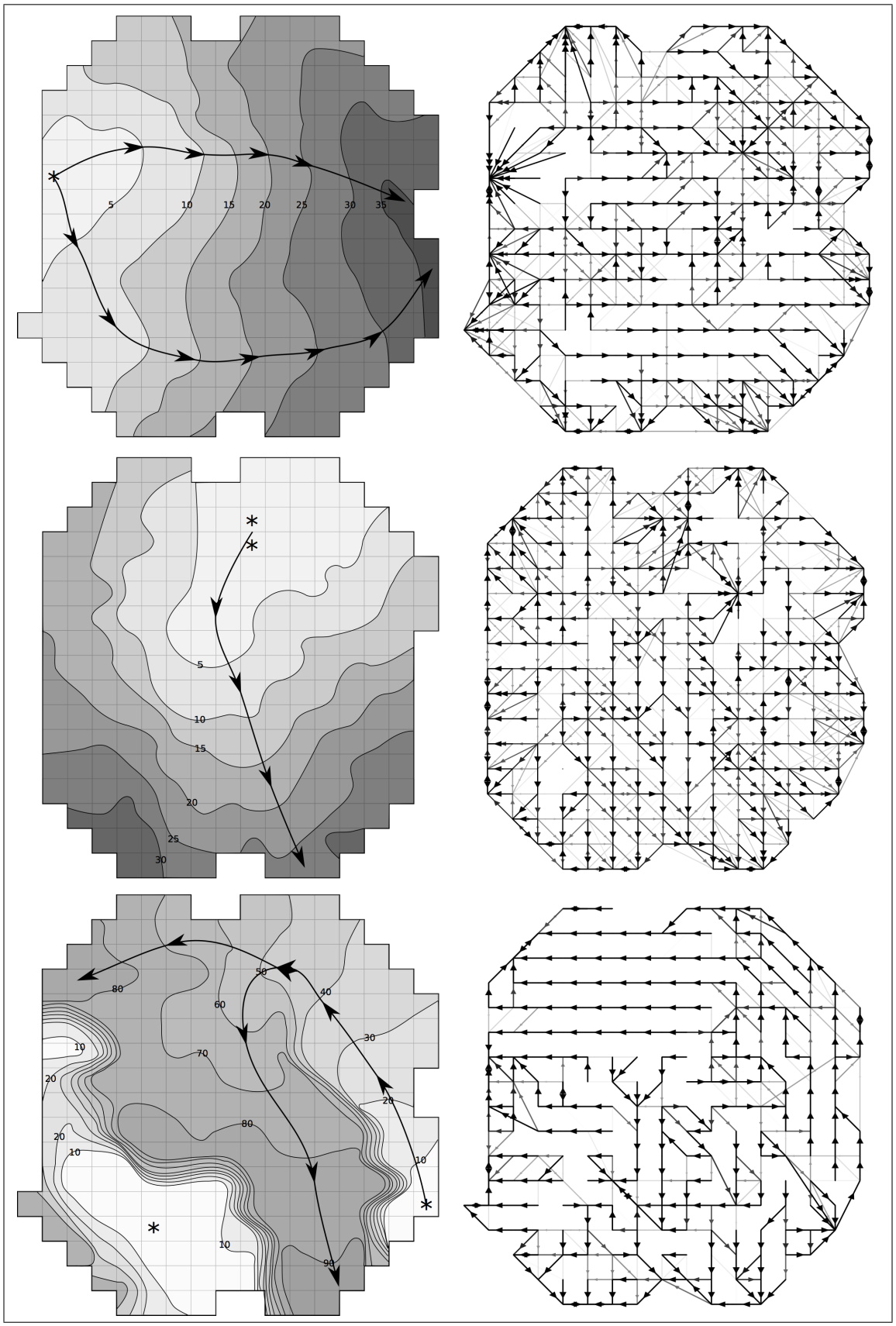

Fig. 1. Isochrone contour maps depicting a single occurrence of three recurring patterns of AF (left) and graphs showing estimated dominant electrode interactions (right). The asterisk (*) marks the starting point of a wavefront in the contour map. The wavefront trajectories are indicated by the bold directed lines. The directed electrode interaction graphs are constructed by drawing a line between electrodes where dominant interactions occur. The strength of the interaction is indicated by a grayscale and width, ranging from black and thick (strong) to white and thin (weak).

recordings were chosen to investigate the relevance of the sparse multivariate regression approach: 1) an ST goat with a large peripheral wavefront, entering the mapping array at the same location and recurring with the same pattern for several seconds, 2) an ST goat with a recurring breakthrough wavefront pattern, and 3) an ST goat with a recurring rotating wavefront pattern.

III. Results

The MVAR model was estimated on 3 second recordings segmented into consecutive 100ms intervals ($M = 100$) with 50ms overlap. Model delay and order were set at $\delta = 1$ and $P = 11$, corresponding to 1ms and 11ms respectively. These values are based on the assumption that local conduction velocity between two horizontally or vertically adjacent electrodes can be as slow as 0.2mm/ms ($^{2.4}/_{0.2} = 12$ms) and should not be faster than 1.5mm/ms ($^{2.4}/_{1.5} = 1.6$ms). The value of the decay factor λ was set at 10mm. Dominant electrode interaction graphs were reconstructed by normalizing the outgoing mean interactions for each electrode to the interval $[0, 1]$ and selecting only interactions with a normalized value higher than 0.75. Fig. 1 shows three examples of identified recurring wave propagation patterns.

1) Peripheral wave train: The top isochrone map and interaction graph in Fig. 1 show the analysis of a recurring pattern of a peripheral wavefront entering from the left, moving from left to right and leaving the mapping area at the right. The contour map on the left shows one such wave, with higher conduction velocity at the top and bottom of the mapping array and slower conduction in the middle. The direction of the wavefront pattern is captured by the dominant interaction graph, where the top and bottom of the mapping array show clear rightward conduction patterns while the pattern in the middle is more diverse. Surprisingly the points where the wavefront enters the mapping area on the left are identified as sinks with many dominant incoming interactions. This can be explained by the observation that at an electrode where a wavefront originates there is no preceding activation at the surrounding electrodes, but they do contain later activations that still correlate with the activation at the originating electrode. At points where a wavefront has just passed, there will be a number of correlating similar activations before and after the front, but for a point where waves originate or come in, only correlations after the front are possible. When the two sides (before and after) are present, the resulting dominant interaction is likely not as strong as when only one side is present. Therefore at sources (just as at sinks) dominant interactions will more easily be pointed towards them. In this case the auto-interaction coefficient a_{ii} can provide additional information.

2) Repetitive breakthrough wave: The middle map and graph in Fig. 1 show a repetitive breakthrough wave pattern, where a wavefront originates from a deeper layer of the atrium. The activation breaks through in the right upper corner of the mapping array and subsequently shows radial spread of activation, leaving the mapping array at the left, bottom and right side. The dominant interaction graph again captures this breakthrough pattern. The upper right part of the interaction graph shows a more complex pattern, again with several electrodes that act as sinks. These electrodes are the locations where most breakthrough waves tend to enter the mapping area.

3) Rotating wave: The bottom map and graph in Fig. 1 depict the pattern of a rotating wave that enters the mapping area in the lower right, moves upward and then turns left. One part of the wavefront leaves the mapping area on the upper left, the other part keeps on turning anticlockwise to return to the point where the wavefront entered the area. The dominant interaction graph clearly shows the first upward movement of the wavefront, the left turn and the leftward exit of the wavefront. The second part of the wavefront is less clear, although several downward paths can be distinguished in the middle and lower part of the mapping area. This can be explained by the fact that the second part of the wavefront is not as recurrent as the first part.

IV. Discussion and Conclusions

The three examples illustrate the identification of recurrent wave propagation patterns using a sparse multivariate regression model. Without the need for annotation and including only a limited amount of underlying assumptions, the developed method is able to capture the relevant dominant interactions between electrograms located at different recording locations. The distance-weighted version of the basis pursuit algorithm is a fast and promising tool to identify interactions within a short timeframe. The constructed dominant interaction graph can be further analyzed using graph theoretical algorithms to identify sources and sinks related to wave propagation, to compute maximum flow between different locations in the mapping array and to quantify graph connectivity. In a clinical setting a real-time implementation of the pattern identification algorithm might be used to guide the ablation process by identification of specific conduction patterns as ablation targets and for verification of conduction block.

References

[1] U. Richter, L. Faes, F. Ravelli, and L. Sörnmo, Propagation Pattern Analysis During Atrial Fibrillation Based on Sparse Modeling, IEEE Transactions on Biomedical Engineering, vol. 59 (5), pp. 1319-1328, 2012.

[2] S. S. Chen, D. L. Donoho, and M. A. Saunders, Atomic Decomposition by Basis Pursuit, SIAM Review, vol 43 (1), pp. 129-159, 2001.

[3] J. J. Fuchs, On sparse representations in arbitrary redundant bases, IEEE Transactions on Information Theory, vol 50, (6), pp.1341-1344, 2004.

[4] D. L. Donoho, M. Elad, On the stability of the basis pursuit in the presence of noise, Signal Processing, vol 86 (3), pp. 511-532, 2006.

[5] S. Verheule, E. Tuyls, A. van Hunnik, M. Kuiper, U. Schotten, and M. Allessie, Fibrillatory Conduction in the Atrial Free Walls of Goats in Persistent and Permanent Atrial Fibrillation, Circulation: Arrhythmia and Electrophysiology, vol 3 (6), pp. 590-599, 2010.

[6] T.S. Söderström and P. Stoica, System Identification, Prentice-Hall, 1989.